Engineering amino acid-derived malonyl-CoA pathways to boost polyketide production in *Yarrowia lipolytica*

Jinpeng Wang[1,2#], Yuxiang Hong[1,3#], Zizhao Wu[1,4], Ayelet Fishman[2], Peng Xu[1,4,5*]

[1]Department of Chemical Engineering, Guangdong Technion-Israel Institute of Technology (GTIIT), Shantou, Guangdong 515063, China

[2]Department of Biotechnology and Food Engineering, Technion-Israel Institute of Technology, Haifa, 3200003, Israel

[3]The Ruth and Bruce Rappaport Faculty of Medicine, Technion-Israel Institute of Technology, Haifa 320002, Israel

[4]Department of Chemical Engineering, Technion – Israel Institute of Technology, Haifa 32000, Israel

[5]Center for Lipid Engineering, Muyuan Laboratory, Zhengzhou, Henan 450016, China

*Corresponding author. P.X. (peng.xu@gtiit.edu.cn or peng.xu@technion.ac.il)

[#]These authors contribute equally to this article.

Abstract

Malonyl-CoA is a central precursor involved in the synthesis of various bio-based chemicals, including polyketides, fatty acids, and flavonoids. However, the production of these chemicals is often limited by the availability of malonyl-CoA. Based on retrosynthesis principles, we designed two thermodynamically favorable malonyl-CoA pathways using L-glutamate and L-aspartate as substrates. The novel pathways leverage oxidative deamination and decarboxylation reactions and efficiently channel metabolic flux toward malonyl-CoA, resulting in increased production of total polyketides beyond the capacity of the native acetyl-CoA carboxylase route using glucose as substrate. We also discovered a new-to-nature polyketide (4-hydroxy-6-hydroxyethyl-2-pyrone) derived from the side activity of the TAL pathway, reaching 6.4 g/L in *Y. lipolytica*. This work highlights the utility of the novel malonyl-CoA pathways in enhancing polyketide production, and the possibility of upcycling abundant amino acids or protein waste in the animal farming or meat industry to produce high-value nonnatural polyketides.

Keywords: Polyketides, Malonyl-CoA, L-Glutamate, L-Aspartate, Metabolic engineering, *Yarrowia lipolytica*

Highlights:

- Two thermodynamically favorable malonyl-CoA pathways in *Yarrowia lipolytica* using L-glutamate and L-aspartate as substrates were engineered.
- The novel oxygen-dependent malonyl-CoA pathways outperformed the canonical acetyl-CoA carboxylase pathway in polyketide production.
- A new-to-nature polyketide, 4-hydroxy-6-hydroxyethyl-2-pyrone (HHEP), was produced at a remarkably high titer of 6.4 g/L in shaking flask.
- The engineered pathway improved the total production of malonyl-CoA-derived compounds (TAL, HHEP, and lipids).

1. Introduction

Malonyl-CoA is the C_2 building block in the biosynthetic pathway of fats (*1, 2*), oleochemicals (*3*), and polyketides (*4-6*) in nature. As such, it sits at the heart of central metabolism in both prokaryotes and eukaryotes and underpins a vast range of biochemical transformations. Beyond its well-known role in fatty acid biosynthesis, malonyl-CoA is also integral to the biosynthesis of numerous high-value compounds including flavonoids (*7, 8*) and many pharmaceutically relevant polyketides (*9-13*). Consequently, boosting intracellular malonyl-CoA availability has become a central goal in metabolic engineering (*14, 15*).

Given malonyl-CoA's central importance, the quest for efficient and feasible malonyl-CoA pathways has long been a focus of the metabolic engineering community. The canonical route relies on pyruvate dehydrogenase (PDH) converting pyruvate into acetyl-CoA, followed by acetyl-CoA carboxylase (ACC) converting acetyl-CoA into malonyl-CoA (**Fig. 1**) (*16*). Although widely employed in industrial microorganisms, this PDH–ACC pathway carries a moderate overall negative Gibbs free energy ($\Delta_r G^{m}$ ≈ –51 kJ/mol) yet also entails high ATP consumption (**Table 1**). A second strategy uses malonyl-CoA synthetase (MCS) (*17-19*) to directly activate malonate into malonyl-CoA ($\Delta_r G^{m}$ ≈ –53.4 kJ/mol), avoiding the carboxylation step and offering kinetic advantages due to simpler enzyme regulation. However, the cost of malonate is economically prohibitive (8,000$/ton). This route also imposes the cells high consumption of ATP. Recently, an alternative "transaminase–malonyl-CoA reductase" route (Fig. 1) was introduced to improve polyketide synthesis (*20*) in *E. coli*, wherein malonate semialdehyde (arising via transamination from β-alanine) is converted to malonyl-CoA by a specialized malonyl-CoA reductase. Although Gibbs energy for this emerging pathway ($\Delta_r G°$ ≈ –16 kJ/mol for the enzyme cascade) can be favorable under standard conditions (species concentration of 1 M), the standard Gibbs free energy under physiologically-relevant conditions ($\Delta_r G^{m}$ ≈ +0.6 kJ/mol, species concentration of 1 mM) is thermodynamically unfavorable. In addition, existing enzyme pairs of transaminase and reductase demonstrated mediocre K_m and k_{cat} values. This necessitates us to find alternative malonyl-CoA pathways to improve microbial production of important metabolites.

An ideal malonyl-CoA pathway should offer greater thermodynamic favorability, improved catalytic constants, or less stringent cofactor and ATP requirements. In this study, we addressed this challenge by retro-synthetically designing and implementing

two novel malonyl-CoA routes, starting from the abundant amino acids L-glutamate and L-aspartate (Fig. 1). Both pathways leverage malonate semialdehyde as the intermediate and malonyl-CoA reductase as a key step. Using the simplest polyketide TAL as a test molecule, we experimentally validated that these new pathways efficiently redirect carbon flux toward malonyl-CoA and boosted TAL and a new-to-nature (4-hydroxy-6-hydroxyethyl-2-pyrone) polyketide production in *Y. lipolytica*. Our re-designed malonyl-CoA pathways expanded the biotechnological repertoire of high-value polyketides from low-cost and abundant amino acids.

2. Results and discussion

2.1 Designing novel oxygen-dependent malonyl-CoA pathways from two abundant amino acids

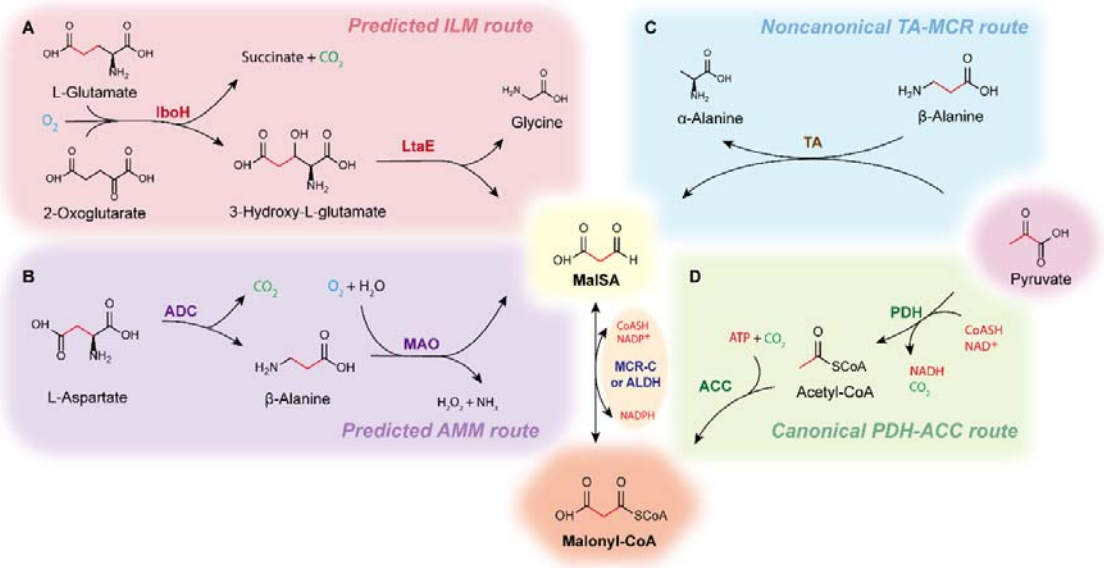

Fig. 1 Malonyl-CoA canonical, noncanonical, and predicted pathways: **(A)** Novel O_2-dependent malonyl-CoA pathways derived from L-glutamate (ILM route). IboH: 2-oxoglutarate-dependent L-glutamate dioxygenase; LtaE: aldolase; MCR-C: malonyl-CoA reductase C-terminal; **(B)** Novel O_2-dependent malonyl-CoA pathways derived from L-aspartate (AMM route). ADC: aspartate decarboxylase, MAO: monoamine oxidase; **(C)** Noncanonical TA-MCR route involves malonate semialdehyde (MalSA). TA: transaminase; **(D)** Canonical PDH-ACC route. PDH: pyruvate dehydrogenase, ACC: acetyl-CoA carboxylase.

We began by applying a retrosynthetic framework to identify possible malonyl-CoA pathways from two abundant amino acids, L-glutamate and L-aspartate. Both proposed pathways generate malonate semialdehyde (MalSA) as an intermediate and then employ malonyl-CoA reductase (MCR) to convert MalSA to malonyl-CoA (**Fig. 1A** and **1B**). In the L-glutamate route, L-glutamate dioxygenase (IboH) (*21*) hydroxylates L-glutamate to form 3-hydroxy-L-glutamate, which subsequently undergoes an aldol cleavage (*22*), yielding MalSA and glycine. In the L-aspartate route, aspartate decarboxylase (ADC) converts L-aspartate to β-alanine (*23*), then β-alanine undergoes an oxidative deamination to form MalSA by a monoamine oxidase (MAO) (*24*), generating hydrogen peroxide (H_2O_2) as byproduct. Both enzymes rely on oxidative deamination and decarboxylation steps releasing CO_2, amine (or glycine) or H_2O_2, proceeding with increased entropy or disorder, signifying a strong driving force or large negative Gibbs energy change.

With an AI-powered kinetic data prediction tool UniKP (*25*) including reported kinetic data, and biochemical reaction thermodynamic calculator *eQuilibrator 3.0* (*26*), we retrieved the kinetic and thermodynamic information of the novel malonyl-CoA pathways. Compared to the canonical PDH-ACC and MCS routes, both the L-glutamate and L-aspartate pathways exhibit reduced ATP demand (**Table 1**), thereby imposing less cellular energy cost. Thermodynamic and kinetic analyses (**Table 2**) indicate that although both pathways rely on MCR — known to exhibit marginal thermodynamic favorability on its own, the large driving force by coupling with oxidative deamination and decarboxylation steps will thermodynamically benefit MCR. Specifically, IboH-aldolase (Δ_rG^m ≈ -466.6 kJ/mol) or ADC-MAO (Δ_rG^m ≈ -146.3 kJ/mol) reactions each display large negative Gibbs free energy changes (**Table 2**), which collectively drive the overall pathway into a highly exergonic regime even when the MCR step by itself is relatively less favorable (*27-29*). This thermodynamic synergy sets our proposed pathways apart from the previously reported transaminase-MCR approach (*20*), whose net Gibbs energy under physiological conditions becomes slightly positive (Δ_rG^m ≈ +0.6 kJ/mol). Moreover, predicted K_m and k_{cat} values for IboH, aldolase, MAO, and MCR, fall within ranges better suitable for metabolic engineering (**Table 2**), than the transaminase-MCR route (*20*).

2.2 Novel malonyl-CoA pathways boost TAL production and produce an unknown metabolite

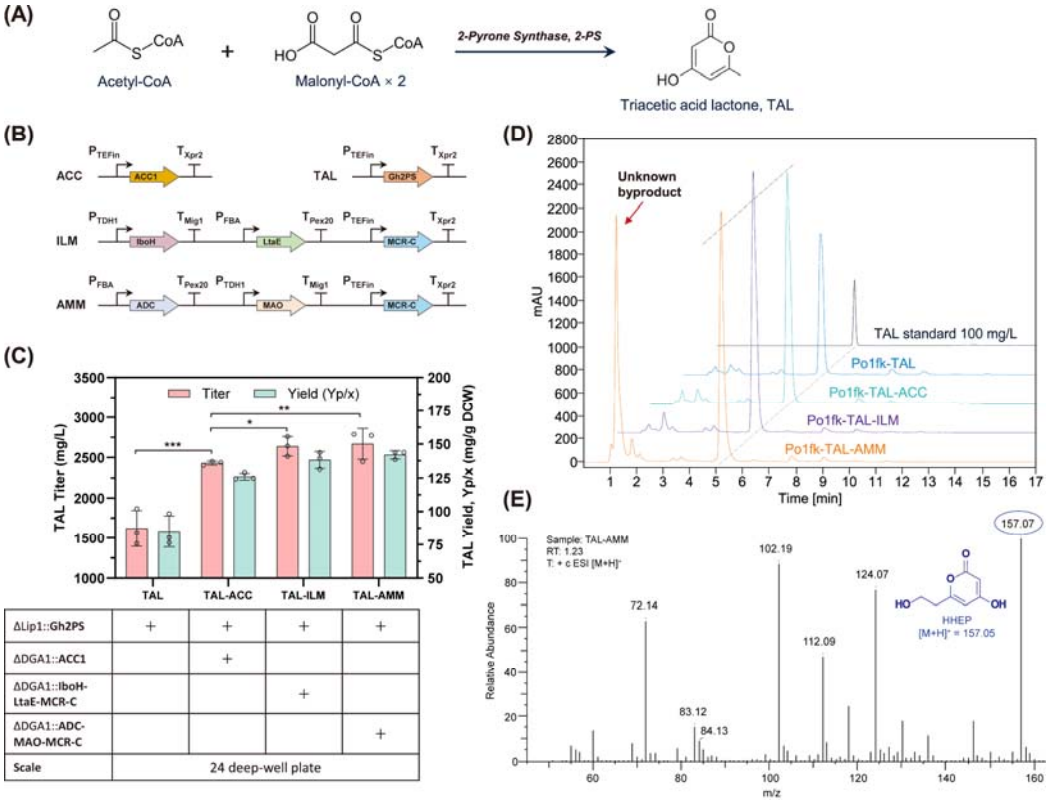

Fig. 2 Testing the functionality of the novel malonyl-CoA pathways. (**A**) The simplest polyketide pathway encoded by 2-pyrone synthase (2-PS) was used as a reporter molecule; (**B**) Three TAL pathways, TAL-ACC, TAL-ILM, and TAL-AMM tested in this work; (**C**) TAL titer and specific TAL yield from the engineered strains in deep-well plates using YPD80 medium. Experiments were performed in triplicate, and the data is reported as mean ± SD. *** indicates statistically highly significant ($p < 0.001$), ** indicates statistically significant ($p < 0.01$), * indicates statistically significant ($p < 0.05$); (**D**) HPLC profile of TAL and an unknown by-product from the engineered strains; (**E**) LC-MS spectra of the unknown metabolite from the TAL-AMM strain.

We next validated whether the novel malonyl-CoA pathways could enhance malonyl-CoA level. Since intracellular malonyl-CoA or its intermediate MalSA are highly unstable, prone to rapid fluctuations, and tightly regulated within central carbon metabolism, we instead employed more stable malonyl-CoA derivatives to assess the activity of these two pathways. Here, *Y. lipolytica* was chosen as the host strain due to its naturally high malonyl-CoA flux, which favors the biosynthesis of polyketides and lipids. Therefore, the simplest polyketide (triacetic acid lactone) was chosen as the test molecule. We integrated a codon-optimized 2-pyrone synthase

156 (*Gh*2PS) from *Gerbera hybrida* into the *lip1* locus of *Y. lipolytica* Po1fk (*30, 31*). This
157 enzyme catalyzes the condensation of malonyl-CoA with acetyl-CoA (**Fig. 2A**) to form
158 triacetic acid lactone (TAL), serving as a direct reporter for the newly designed
159 malonyl-CoA pathways. The Lip1 gene, encoding a lipase involved in triglyceride
160 hydrolysis, was chosen to prevent the degradation of storage lipids and the
161 subsequent generation of acetyl-CoA for β-oxidation pathway, which could confound
162 the interpretation of flux through our engineered pathways. To compare the
163 performance of the novel pathways, we constructed three different strains (**Fig. 2B**)
164 by integrating either ACC1 (canonical pathway), the ILM pathway (IboH-LtaE-MCR-C,
165 using L-glutamate as substrate, **Fig. 1A**), or the AMM pathway (ADC-MAO-MCR-C,
166 using L-aspartate as substrate, **Fig. 1B**) into the *DGA1* locus under well-defined
167 promoters (Fig. 2B). The DGA1 gene, encoding a diacylglycerol acyltransferase
168 essential for triglyceride biosynthesis, was chosen as the genome integrated loci to
169 divert malonyl-CoA flux away from lipid synthesis and toward polyketide production.

170 TAL production in deep-well plate cultures (**Fig. 2C**) indicates that both ILM and
171 AMM pathways outperformed the canonical ACC1 route in terms of titer and specific
172 yield (mgTAL/gDCW). Specifically, the strain carrying the ILM pathway achieved a TAL
173 titer of 2638.8 mg/L, while the AMM pathway led to a slightly higher TAL titer of
174 2669.6 mg/L (**Fig. 2C**), both exceeding the ACC1 control (2431.1 mg/L). This suggests
175 that the oxidative deamination and decarboxylation steps in the novel pathways (**Fig.**
176 **1**) effectively converted the amino acid precursors into malonyl-CoA, overcoming the
177 inherent limitations of ATP-dependent carboxylation in the ACC1 pathway (**Table 1**).
178 The higher TAL yield observed in the AMM pathway could be attributed to a more
179 favorable kinetic profile of the ADC-MAO cascade (**Table 2**).

180 Interestingly, HPLC analysis revealed an unknown by-product in the strain
181 carrying the AMM pathway (**Fig. 2D**). This unknown peak persists in the shaking flask
182 culture (supplementary **Fig. S1B**). Moreover, in shaking flasks, AMM strain produced
183 less TAL than the strain carrying ILM pathway (supplementary **Fig. S1A**), possibly due
184 to competition from an unknown by-product that accumulates in the AMM pathway
185 (supplementary **Fig. S1B**). This byproduct is likely derived from the β-alanine or
186 MalSA intermediates. We next identified the structure of the unknown metabolite
187 (**Fig. 2D**) observed in the AMM strain. LC–MS analysis (**Fig. 2E**) revealed a major
188 species eluting at 1.26 min (supplementary **Fig. S2**), with a molecular weight of
189 157 Dalton and characteristic fragmentation ions at *m/z* = 124, 112, 102, 84 and 72
190 under positive (M+1) ionization modes. By comparing these fragmentation patterns
191 against standard databases and predicted mass spectra (supplementary **Fig. S3**), we

characterized this molecule as 4-hydroxy-6-hydroxyethyl-2-pyrone (HHEP) with a chemical formula $C_7H_8O_4$.

2.3 3-HP-CoA serves as the priming unit for the nonnatural polyketide HHEP

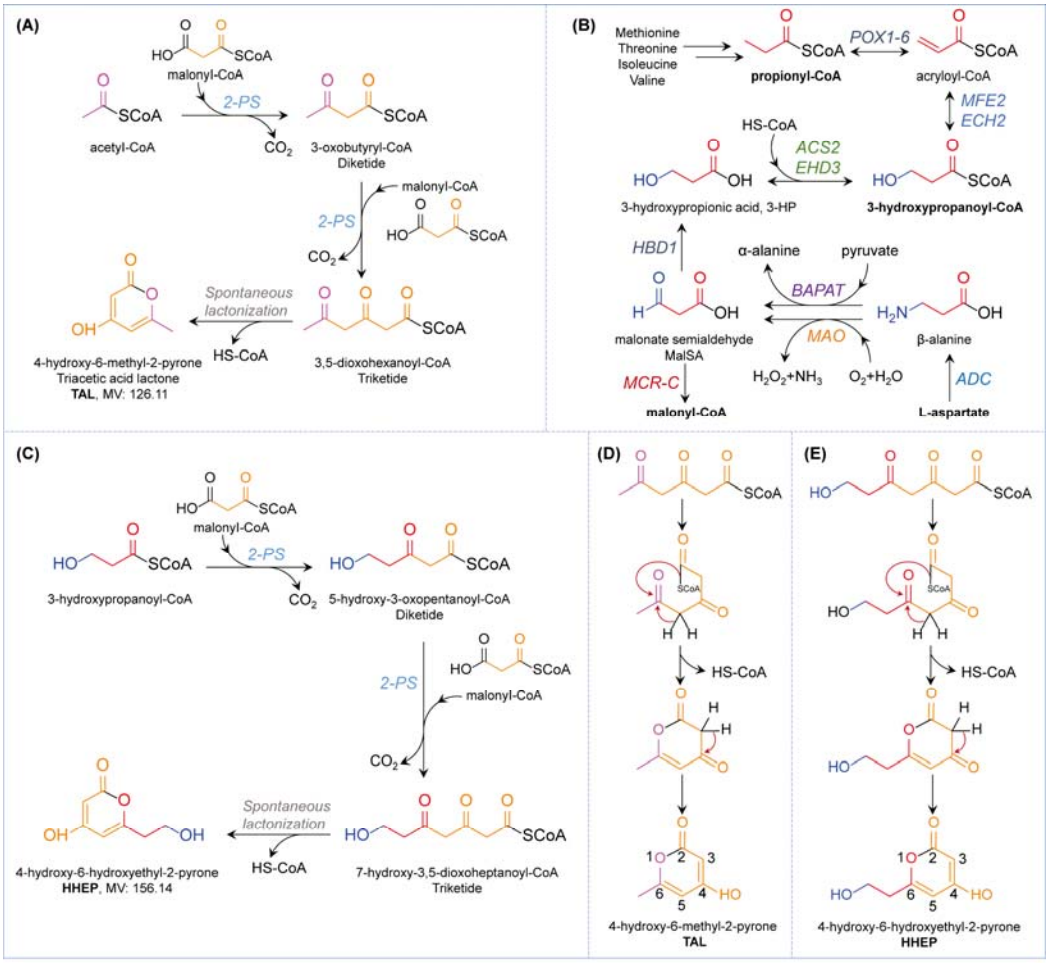

Fig. 3. Deciphering the biosynthetic route of the nonnatural polyketide HHEP. (**A**) Biosynthetic route of TAL by 2PS. (**B**) Generation of 3-HP and 3-HP-CoA from endogenous amino acid metabolism (upper panel) and β-alanine from L-aspartate decarboxylation (lower panel). BAPAT: β-alanine-pyruvate aminotransferase; MAO: monoamine oxidase; HBD1: 3-hydroxyacyl-CoA dehydrogenase; ACS2/EHD3: 3-hydroxypropanoyl-CoA synthetase; POX1-6: Fatty-acyl-CoA oxidase; MFE2: Multifunctional β-oxidation enzyme, hydratase/dehydrogenase; ECH2: Enoyl-CoA hydratase. (**C**) 3-HP-CoA serves as a priming molecule to synthesize HHEP by 2PS. Spontaneous lactonization of triketide intermediates leads to the formation of triacetic acid lactone (**D**) and 4-hydroxy-6-hydroxyethyl-2-pyrone (**E**).

207 Previously, the β-alanine pathway has been identified as the most economically
208 attractive route to synthesize 3-hydroxypropionate (3-HP) (*32*). Inspection of TAL
209 biosynthetic mechanism (**Fig. 3A**) led us to hypothesize that HHEP was generated as a
210 polyketide by-product when 3-hydroxypropanoyl-CoA (3-HP-CoA) was used as an
211 alternative priming molecule for 2-pyrone synthase (2PS) (**Fig. 3B** and **3C**) (*33*). In the
212 AMM strain, β-alanine generated from aspartate decarboxylase (ADC) can be
213 oxidized to form MalSA, which further is reduced to 3-HP by host enzyme HBD1
214 encoding 3-hydroxyacyl-CoA dehydrogenase (**Fig. 3B** lower panel). In fact, 3-HP-CoA
215 is also the degradation product of methionine, threonine, leucine, and valine (**Fig. 3A**
216 upper panel) from the media containing YPD and peptone. When we blasted the
217 genome of *Y. lipolytica*, we identified that at least one gene (YALI0D06325) encodes
218 an enzyme highly conserved with BAPAT encoding alanine aminotransferase which
219 converts β-alanine to MalSA (supplementary **Fig. S6**); and likewise, YALI0C08811 and
220 YALI0F05962/YALI0D06215g are highly conserved with HBD1 encoding 3-hydroxyacyl-
221 CoA dehydrogenase, and ACS2/EHD3 encoding 3-hydroxypropanoyl-CoA synthetase
222 (supplementary **Fig. S7-S9**), respectively. Theoretically, when 2PS encounters 3-HP-
223 CoA as a priming unit, it could condense with two molecules of malonyl-CoA to form
224 a hydroxymethyl triketide intermediate (**Fig. 3C**). This intermediate, undergoes a
225 series of intramolecular nucleophilic substitutions and spontaneous lactonization,
226 ultimately cyclizes and rearranges to yield the more stable lactone
227 4-hydroxy-6-hydroxyethyl-2-pyrone (HHEP) (**Fig. 3E**) following a similar pattern as 4-
228 hydroxy-6-methyl-2-pyrone (TAL) (**Fig. 3D**) does. Interestingly, we found HHEP was
229 synthesized in all the strains expressing 2PS (**Fig. 2D**, supplementary **Fig. S4** for ILM-
230 TAL strain and supplementary **Fig. S5** for TAL strain), albeit HHEP was mostly
231 accumulated in the AMM strain (supplementary **Fig. S1B** and **Fig. S2**). The non-
232 exclusive production of HHEP from all the tested strains suggests that the primer unit,
233 3-HP-CoA, is derived at low levels from the degradation of branched-chain amino
234 acids (e.g., valine, methionine, threonine) (**Fig. 3B** upper panel) or generated from
235 the reduction of MalSA via β-alanine metabolism (**Fig. 3B** lower panel).

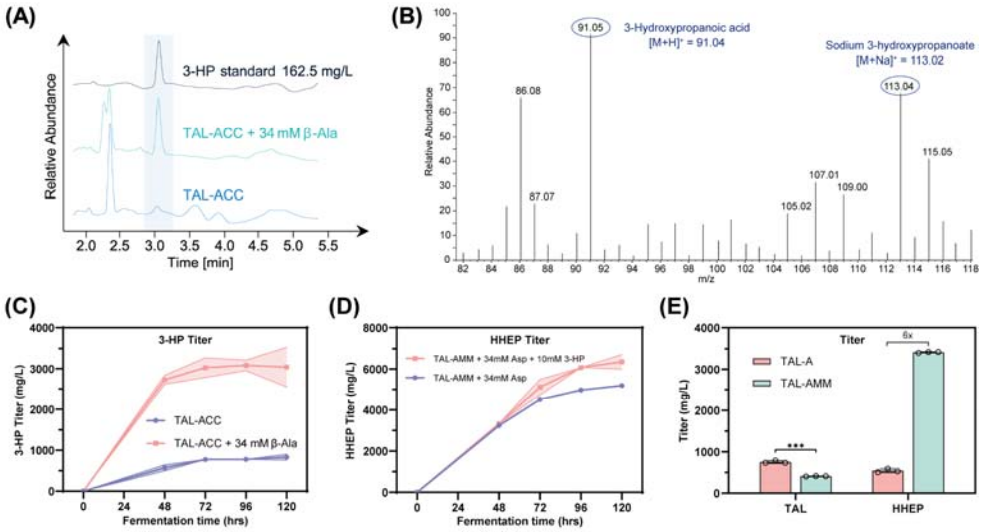

Fig. 4 Validating 3-HP as an intermediate for HHEP synthesis. (**A**) HPLC profile of 3-HP in the TAL-ACC strain with feeding of 34 mM β-alanine; (**B**) LC-MS characterization of 3-HP in the TAL-ACC strain; (**C**) Production of 3-HP in the TAL-ACC strain with or without feeding of 34 mM β-alanine in shaking flask using YPD80 medium. β-Ala feeding: 5 mM, 5 mM, 8 mM, 8 mM, and 8 mM were added at 24 h, 36 h, 48 h, 60 h, and 72 h, respectively, resulting in a total supplement of 34 mM; (**D**) Production of HHEP in the TAL-AMM strain with or without feeding of 10 mM 3-HP in shaking flask using YPD80 medium. 3-HP feeding: 1.4 mM, 1.4 mM, 2.4 mM, 2.4 mM, and 2.4 mM were added at 24 h, 36 h, 48 h, 60 h, and 72 h, respectively, resulting in a total supplement of 10 mM. L-Aspartate feeding: 5 mM, 5 mM, 8 mM, 8 mM, and 8 mM were added at 24 h, 36 h, 48 h, 60 h, and 72 h, respectively, resulting in a total supplement of 34 mM; (**E**) TAL and HHEP production in the TAL-A and TAL-AMM strain after 48 hours of fermentation in deep-well plates using YPD80 medium. TAL-A is the strain with expression of 2PS and ADC. TAL-AMM is the strain with expression of 2PS and the entire AMM pathway.

To validate that HHEP is derived from 3-HP, we next fed 34 mM β-alanine to the TAL-ACC strain and observed a substantially increased level of 3-HP in shaking flask (Fig. **4A** and supplementary **Fig. S10A**). The presence of 3-HP was also confirmed by LC-MS analysis (**Fig. 4B**). For example, TAL-ACC strain produced 3042.0 mg/L of 3-HP with feeding of 34 mM β-alanine, more than 3-fold higher than the same strain without feeding of β-alanine (831.8 mg/L) (**Fig. 4C** and supplementary **Fig. S10A**). These facts confirm that endogenous BAPAT (YALI0D06325) and HBD1 (YALI0C08811)

260 can convert β-alanine to 3-HP (**Fig. 3B**). To directly validate that HHEP is derived from
261 3-HP-CoA, we next fed TAL-AMM with 34 mM of 3-HP. However, the addition of 34
262 mM 3-HP was found to inhibit cell growth, likely due to its inherent toxicity
263 (supplementary **Fig. S11A**). Therefore, we reduced the 3-HP supplementation to 10
264 mM, while simultaneously supplying 34 mM L-aspartate to ensure sufficient malonyl-
265 CoA availability for the condensation of 3-HP-CoA and malonyl-CoA into HHEP. The
266 results demonstrated that feeding 10 mM 3-HP significantly increased the HHEP titer
267 to 6359.1 mg/L, which is 22.5% higher than that of the non-fed group (5191.3 mg/L)
268 (**Fig. 4D** and supplementary **Fig. S11C**). These findings confirm that the endogenous
269 3-hydroxypropanoyl-CoA synthetase can activate 3-HP to 3-HP-CoA for the synthesis
270 of the polyketide HHEP (**Fig. 3B**). When only ADC was expressed, the TAL-A strain
271 produced basal level of TAL (751.0 mg/L) and HHPE (542.4 mg/L) (**Fig. 4E** and
272 supplementary **Fig. S10B**). However, when the entire AMM pathway was expressed,
273 the TAL-AMM strain produced 6-fold more HHPE (3415.1 mg/L) compared to the TAL-
274 A strain (**Fig. 4E** and Supplementary **Fig. S10C**). This result showcases the critical roles
275 of monoamine oxidase (MAO) and MCR to boost intracellular malonyl-CoA and
276 improve HHEP synthesis (**Fig. 3B** and **Fig. 3C**). The discrepancy of TAL and HHEP titer
277 enhancement indicates the intracellular scarcity of acetyl-CoA relative to 3-
278 hydroxypropanoyl-CoA in the TAL-AMM strain, alternatively, 2PS may prefer 3-HP-
279 CoA over acetyl-CoA as the priming molecule. Taken together, these results confirm
280 that HHEP arises as a nonnatural polyketide by-product when 3-HP-CoA participates
281 in the 2-PS condensation reaction (**Fig. 3B** and **Fig. 3C**).

282 HHEP is a structural analog of the natural product Kojic acid, which is a well-
283 known whitening and skincare natural product. This is the first report on the
284 synthesis of the nonnatural polyketide HHEP, and the biological activity of HHEP has
285 yet to be discovered. Furthermore, HHEP holds promise as a versatile bio-based
286 platform compound. It could serve as a precursor for the synthesis of functional
287 polymers, including biodegradable polyesters and UV-curable resins, through
288 esterification or oxidative modification. In addition, the conjugated system may
289 enable its application as an antioxidant, UV-absorbing, or cross-linkable additive in
290 coatings and materials. These properties suggest that HHEP represents a valuable
291 compound for developing sustainable, high-value chemicals and polymeric materials.

292 **2.4 Feeding amino acids to boost polyketide and lipid production in shaking flask**

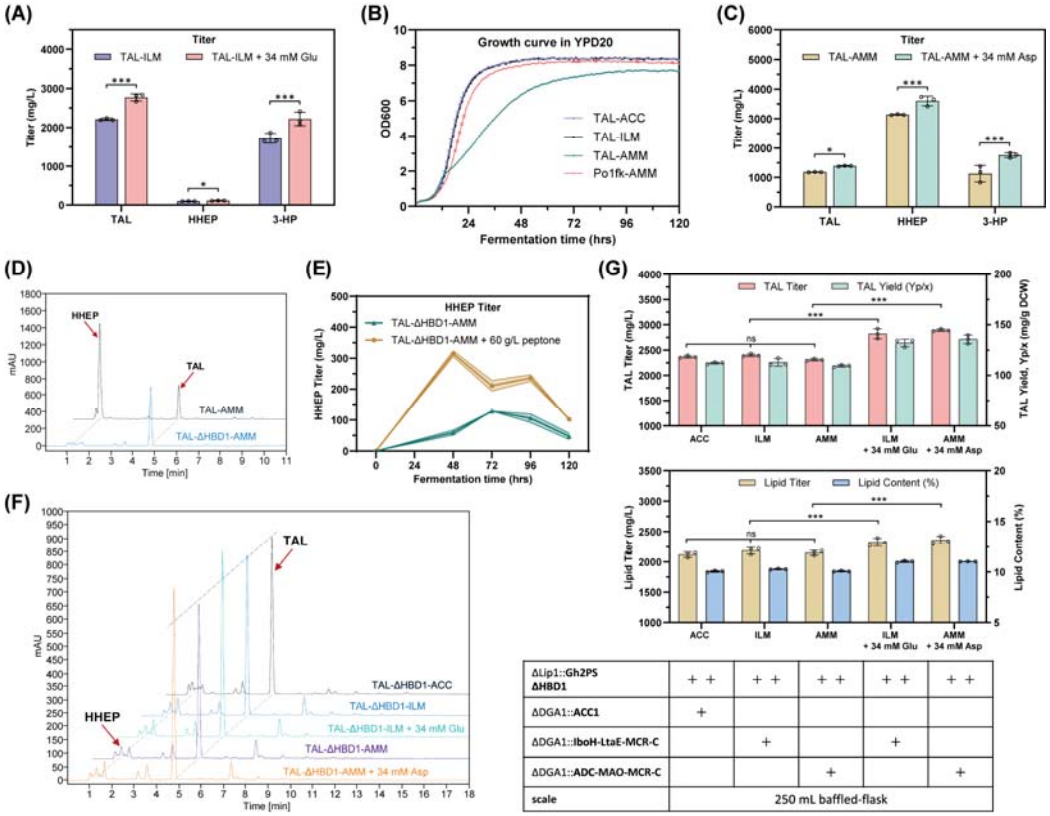

ΔLip1::Gh2PS ΔHBD1	+ +	+ +	+ +	+ +	+ +
ΔDGA1::ACC1	+				
ΔDGA1::IboH-LtaE-MCR-C		+		+	
ΔDGA1::ADC-MAO-MCR-C			+		+
scale	250 mL baffled-flask				

Fig. 5. Feeding L-glutamate or L-aspartate to improve polyketide production in TAL-ILM or TAL-AMM strain. (**A**) TAL, HHEP and 3-HP production in TAL-ILM strain with or without feeding 34 mM L-glutamate in 250 mL baffled-flask using YPD80 medium. L-Glutamate feeding: 5 mM, 5 mM, 8 mM, 8 mM, and 8 mM were added at 24 h, 36 h, 48 h, 60 h, and 72 h, respectively, resulting in a total supplement of 34 mM; (**B**) Growth fitness of HHEP-producing strain (TAL-AMM) is reduced compared to other TAL-producing strain; (**C**) TAL, HHEP and 3-HP production in TAL-AMM strain with or without feeding of 34 mM L-aspartate in 250 mL baffled-flask using YPD80 medium. L-Aspartate feeding: 5 mM, 5 mM, 8 mM, 8 mM, and 8 mM were added at 24 h, 36 h, 48 h, 60 h, and 72 h, respectively, resulting in a total supplement of 34 mM; (**D**) HPLC profile show that the HHEP peak returned to basal level almost undetectable when HBD1 gene was deleted; (**E**) Production of HHEP in the TAL-ΔHBD1-AMM strain with or without feeding of 60 g/L peptone in shaking flask using YPD80 medium. Peptone feeding: 10 g/L, 10 g/L, 10 g/L, 15 g/L, and 15 g/L were added at 24 h, 36 h, 48 h, 60 h, and 72 h, respectively, resulting in a total supplement of 60 g/L; (**F**) HPLC profile of TAL and HHEP from the engineered strains after knocking out HBD1: the product shifts to TAL accumulation; (**G**) TAL titer, specific TAL yield, lipid titer and lipid content from the engineered strains with or without amino acid feeding in 250 mL baffled-

312 flask using YPD80 medium. L-Glutamate or L-aspartate feeding: 5 mM, 5 mM, 8 mM,
313 8 mM, and 8 mM were added at 24 h, 36 h, 48 h, 60 h, and 72 h, respectively,
314 resulting in a total supplement of 34 mM. Experiments were performed in triplicate,
315 and the data is reported as mean ± SD. *** indicates statistically highly significant (p
316 < 0.001), * indicates statistically significant ($p < 0.05$), ns indicates statistically
317 significant ($p > 0.05$).

318

319 We next tested whether feeding L-glutamate or L-aspartate to the ILM and AMM
320 strains will boost malonyl-CoA derivatives production, including TAL, HHEP and lipid.
321 Since our designed pathway is oxygen-dependent, we cultured the ILM strain in
322 shaking flask to improve oxygen supply. After feeding 34 mM L-glutamate to the TAL-
323 ILM strain, both TAL and HHEP titer were increased in the shaking flasks (**Fig. 5A**). TAL
324 yield was increased by 25% compared to the same strain without L-glutamate
325 feeding (supplementary **Fig. S12A** and **Fig. S12D**). This result indicated that feeding
326 with L-glutamate boosted malonyl-CoA pools and polyketide synthesis in the TAL-ILM
327 strain. HHEP instead decreased after 72 hours (supplementary **Fig. S12B**), indicating
328 the possible degradation of HHEP by the host.

329 While cell growth in the TAL-ILM, TAL-ACC and AMM strains remain unchanged;
330 the TAL-AMM strain exhibits pronounced growth-retardation (**Fig. 5B**), possibly due
331 to the inhibitory effect of HHEP. Using TAL as an internal standard, we determined
332 that TAL-AMM strain produced 3140.9 mg/L of HHEP (**Fig. 5C**). After feeding 34 mM
333 L-aspartate to TAL-AMM strain, the production of TAL, HHEP and 3-HP increased by
334 17.4%, 14.7% and 55.5%, respectively (**Fig. 5C** and supplementary **Fig. S13B**). And
335 the total polyketide (both TAL and HHEP) was boosted to 5.0 g/L (**Fig. 5C**), which is
336 more than 1.9-fold of the total polyketides (TAL and HHEP) than the ACC pathway
337 (supplementary **Fig. S1A**).

338 We next deleted HBD1, to eliminate interference from the endogenous 3-HP-
339 CoA-related pathways (**Fig. 3B** and **3C**). Compared to TAL-AMM strain, the TAL-
340 ΔHBD1-AMM strain exhibited significantly lower HHEP production (**Fig. 5D**). However,
341 HHEP was still detectable in all the HBD1 knockout strain (**Fig. 5D**), suggesting that
342 the precursor of HHEP, 3-hydroxypropanoyl-CoA, may also be derived from the
343 endogenous branched-chain amino acid degradation (**Fig. 3B** upper panel). Therefore,
344 we next fed the TAL-ΔHBD1-AMM strain with 60 g/L peptone to provide abundant
345 branched-chain amino acids. As a result, the HHEP titer increased by 1.5-fold
346 compared with cultures grown on YPD medium alone (**Fig. 5E** and supplementary **Fig.**

347 **S14A**). This indicates that 3-HP-CoA derived from branched-chain amino acid
348 catabolism can contribute to the baseline HHEP production across all 2PS-expressing
349 strains. Cell growth fitness analysis (supplementary **Fig. S14B**) further revealed that
350 deletion of HBD1 restored normal growth in the TAL-AMM strain, indicating that
351 HHEP indeed acts as a growth-inhibitory compound. Taken together, removal of
352 HBD1 has allowed for a more straightforward assessment of the pathway's
353 performance by eliminating a major malonyl-CoA competing pathway.

354 To assess the efficiency of different malonyl-CoA pathways, we next constructed
355 three engineered strains based on HBD1-deleted chassis, the TAL-ΔHBD1-ACC strain
356 produced 2368.9 mg/L TAL from glucose, while the ILM and AMM strains yielded
357 2401.4 mg/L and 2310.4 mg/L, respectively. Similarly, the TAL-ΔHBD1-ACC strain
358 produced 2121.9 mg/L lipid from glucose, while the ILM and AMM strains yielded
359 2187.1 mg/L and 2152.0 mg/L, respectively. These results indicate that the ILM and
360 AMM pathways provide malonyl-CoA at a level comparable to that of ACC pathway
361 (**Fig. 5G**). We next fed 34 mM L-glutamate to the ILM strain, TAL production was
362 increased from 2401.4 mg/L to 2822.6 mg/L, and lipid production was increased
363 from 2187.1 mg/L to 2329.0 mg/L. Similarly, feeding 34 mM L-aspartate to the AMM
364 strain raised TAL titer from 2310.4 mg/L to 2893.4 mg/L and lipid titer from 2152.0
365 mg/L to 2356.9 mg/L, representing increases of 25.2% and 9.5%, respectively. (**Fig. 5F**
366 and **Fig. 5G**). These results confirm that the new amino acid-derived malonyl-CoA
367 pathways effectively boost polyketide and lipid production in *Y. lipolytica*.

368 Interestingly, significantly elevated HHEP titers were observed specifically in the
369 TAL-AMM strain (**Fig. 4D**), which may result from the MalSA precursor overflow effect.
370 The TAL-AMM strain generates malonate semialdehyde (MalSA) from two primary
371 sources: engineered MAO and endogenous BAPAT steps (**Fig. 3B** lower panel).
372 Although MCR step is designed to oxidize MalSA to malonyl-CoA, the endogenous
373 HBD1 effectively competes with MCRA pool, reducing MalSA to 3-HP, which is
374 subsequently activated to 3-HP-CoA by EHD3 (Fig. 3B). This creates an abundant
375 supply of the starting unit 3-HP-CoA for 2PS, leading to high-level HHEP synthesis. By
376 deleting HBD1 in the TAL-AMM strain, HHEP production reduced to a level
377 comparable to other 2PS-expressing strains, which 3-HP-CoA can only be derived
378 from the degradation of the branched-chain amino acids in the media (**Fig. 3B** upper
379 panel). In contrast, the TAL-ILM strain only produces MalSA from the aldolase LtaE
380 (**Fig. 1B**), resulting in less 3-HP-CoA formation and consequently lower HHEP titer.

381 **2.5 Feeding L-aspartate to boost polyketide and lipid production in bioreactor**

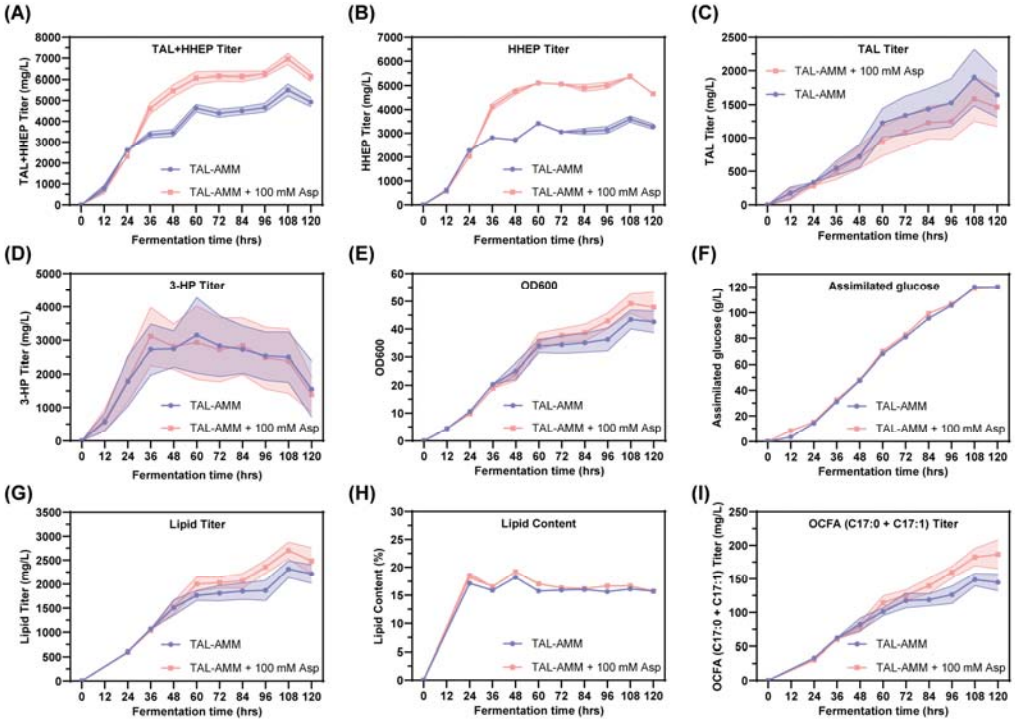

Fig. 6 Feeding L-aspartate to improve polyketide and lipid production in TAL-AMM strain in a 1.0 L mini-bioreactor. TAL+HHEP(**A**), HHEP(**B**), TAL(**C**) and 3-HP(**D**) production in TAL-AMM strain with or without feeding of 100 mM L-aspartate in a 1L bioreactor. L-Aspartate feeding: 5 mM, 10 mM, 15 mM, 15 mM, 15 mM, 20 mM, and 20 mM were added at 0 h, 12 h, 24 h, 36 h, 48 h, 60 h, and 72 h, respectively, resulting in a total supplement of 100 mM; (**E**) Optical density OD600 during fermentation in a 1L bioreactor; (**F**) Amount of glucose consumed during fermentation in a 1L bioreactor; Total Lipid titer (**G**), lipid content (**H**) and total odd-chain fatty acid (OCFA) production in TAL-AMM strain with or without feeding of 100 mM L-aspartate in a 1L bioreactor.

To evaluate the effect of L-aspartate feeding on polyketide production at a larger scale, we conducted a 1 L bioreactor fermentation using the TAL-AMM strain, with or without the addition of 100 mM L-aspartate. The combined titer of TAL and HHEP in the L-aspartate-fed culture reached a peak of 6955.2 mg/L at 108 h, which is a 26.4% increase compared to the maximum titer of 5500.5 mg/L in the control strain without L-aspartate feeding (**Fig. 6A**). This substantial improvement suggests that L-aspartate feeding enhances malonyl-CoA supply toward total polyketide biosynthesis. With L-Asp feeding, HHEP reached a peak of 5368.6 mg/L, representing a 49.2%

402 increase compared to the control group (3597.3 mg/L) (**Fig. 6B**). Notably, HHEP
403 reached 5113.0 mg/L by 60 hours of fermentation, when only 70 g/L of glucose was
404 consumed (**Fig. 6F**). HHEP accumulation slows down after 60 hours, despite
405 continued glucose consumption. This may indicate degradation of the product HHEP.

406 Interestingly, TAL production decreased in the L-aspartate-fed culture compared
407 to the control, particularly after 48 hours (**Fig. 6C**). This suggests that with excess L-
408 aspartate, a greater portion of the precursor malonyl-CoA is channeled toward HHEP
409 biosynthesis rather than TAL accumulation. The increased availability of L-aspartate
410 likely facilitates the formation of the HHEP precursor 3-hydroxypropionyl-CoA (3-HP-
411 CoA), thereby leading to a substantial increase in HHEP. This shift in product
412 distribution reinforces the role of L-aspartate as a flux-enhancing agent that drives
413 carbon flowing through the AMM pathway. Furthermore, the 3-HP titer in the L-
414 aspartate-fed culture peaked at 3119.0 mg/L, equivalent to 3152.2 mg/L maximum in
415 the control strain. Notably, 3-HP production gradually decreased after 60 hours,
416 regardless of whether L-aspartate was fed (**Fig. 6D**). This suggests a shift in metabolic
417 flux from 3-HP to HHEP: 3-HP was converted to 3-HP-CoA promoting an increased
418 flux toward HHEP.

419 Cell growth slightly improved with L-aspartate supplementation, reaching a final
420 OD600 of 49.2, compared to 43.4 in the control (**Fig. 6E**). Despite differences in
421 product profiles, glucose consumption was identical between both conditions, with a
422 total consumption of 120 g/L at the end of fermentation (**Fig. 6F**). This indicates that
423 the observed differences in product titers were not due to changes in glucose uptake
424 but rather due to increased supply of malonyl-CoA through the amino-acid-derived
425 malonyl-CoA pathways.

426 For lipid titer, L-aspartate supplementation led to a consistent increase in total
427 lipid titer throughout the fermentation process (**Fig. 6G**). The maximum lipid titer of
428 the L-Asp supplemented culture reached 2703.7 mg/L, representing a 17.0% increase
429 over the control (2311.6 mg/L). The lipid content (% of cell dry weight) exhibited only
430 a slight increase under L-aspartate feeding, peaking at 19.2% (**Fig. 6H**). This indicates
431 that L-aspartate raises the absolute lipid titer by promoting malonyl-CoA synthesis. In
432 addition, we observed a pronounced increase in odd-chain fatty acid (OCFA; C17:0
433 and C17:1) production following L-aspartate supplementation. The maximum OCFA
434 titer in the supplemented culture reached 186.5 mg/L, compared to 148.9 mg/L in
435 the control, corresponding to a 25.3% increase (**Fig. 6I**, supplementary **Fig. S15A**).
436 This enhancement can be attributed to the ability of L-aspartate to boost the supply
437 of propionyl-CoA, the starting unit for OCFA biosynthesis (**Fig. 3B**). OCFA synthesis

438 also needs malonyl-CoA as the extender units. This finding is consistent with earlier
439 observations that L-aspartate feeding redirects metabolic flux toward the synthesis
440 of polyketide and lipid within the AMM pathway.

441 Together, these results demonstrate that L-aspartate feeding is an effective
442 strategy to enhance high-value polyketide production in engineered *Y. lipolytica*.
443 Both L-aspartate and L-glutamate are among the most abundant amino acids in food
444 and animal farming waste. Different from the reported transaminase-MCR route (*20*),
445 our re-designed malonyl-CoA pathway leverages hydroxylation (in the case ILM) or
446 oxidative deamination (in the case AMM) with oxygen consumption, and therefore it
447 provides a large driving force to compensate the relatively inefficient MCR step.
448 When coupled together, the novel ILM and AMM pathway efficiently converted L-
449 glutamate or L-aspartate to malonyl-CoA and improved the production of both TAL
450 and HHEP. These novel pathways are particularly useful to produce malonyl-CoA-
451 derived compounds under aerobic conditions, potentially benefiting large-scale
452 fermentations. Our results established a promising and scalable polyketide
453 production platform from low-cost amino acid precursors or waste protein streams.
454

455 **3. Conclusions**

456 Herein we have designed and validated two malonyl-CoA biosynthetic pathways
457 in *Y. lipolytica*, utilizing L-glutamate and L-aspartate as substrates. These pathways
458 provide an efficient and ATP-independent alternative for metabolic engineering
459 applications, which expands nature's capacity to produce malonyl-CoA-derived
460 chemicals in *Y. lipolytica*. By leveraging oxidative deamination and decarboxylation
461 reactions, both pathways effectively redirected metabolic flux toward malonyl-CoA,
462 significantly enhancing the biosynthesis of triacetic acid lactone (TAL), a new-to-
463 nature polyketide HHEP, lipid and odd chain-length fatty acids. The strain with AMM
464 pathway produced a novel polyketide HHEP, at 6.4 g/L, highlighting the utility of the
465 amino acid-derived malonyl-CoA pathway and the superior metabolic versatility of *Y.*
466 *lipolytica*. The total polyketide production reached 7.0 g/L in a 1L bioreactor. Our
467 findings demonstrated that low-cost amino acids or protein waste streams could be
468 used as efficient raw materials to manufacture high-value polyketides. The study also
469 reveals thermodynamic coupling could be used to overcome inefficient enzymatic
470 steps. Overall, this work represents an important step toward sustainable and cost-
471 effective production of polyketides by rewiring the amino acid metabolism in
472 microbes.

473 # 4. Materials and methods

474 ## 4.1 Strains and cultural conditions

475 All engineered *Y. lipolytica* strains in this research were derived from Po1fk, a
476 commonly used laboratory strain of *Y. lipolytica* that is leucine- and uracil-
477 prototrophic (Po1g-Δura3-Δku70::loxP). *Escherichia coli* DH5α was cultured in LB
478 medium supplemented with 100 mg/mL ampicillin for plasmid construction and
479 extraction. *Y. lipolytica* strains were cultured in YPD medium for genomic DNA
480 extraction or linearized plasmid transformation. Engineered strains were fermented
481 in YPD-based medium to produce triacetic acid lactone. SD-Ura and SD-Leu plates
482 were used to isolate positive *Y. lipolytica* transformants. The Cre-loxP system was
483 used to eliminate the URA3 selection marker (*34*). To conduct 24-deep-well plates or
484 250 mL shake-flask fermentation, the strain was grown in 3 mL YPD medium for 1 day
485 to prepare a seed culture. A portion of the seed culture was utilized to inoculate 3.5
486 mL or 15 mL of YPD medium with 80 g/L glucose and additional glutamic acid or
487 aspartic acid, with the aim of achieving an initial OD600 value of 0.2, followed by
488 fermentation at 30°C and 250 rpm for 120 h. All engineered strains utilized in
489 fermentation were prototrophic. The formulations of LB medium, YPD medium, SD-
490 Ura plate, SD-Leu plate, and YPD-5-FOA plate were outlined in the supplementary
491 **materials**.

492 ## 4.2 Genetic engineering and strain construction

493 In this research, expression cassette plasmids for individual genes were
494 generated by Gibson assembly and verified by DNA sequencing. Subsequently, we
495 assembled multiple expression cassettes on an integrative vector using a subcloning
496 method of digestion and ligation, following YaliBrick assembly protocols (*35, 36*). All
497 plasmids constructed are listed in the supplementary **Table S1**. The plasmid (*35*) used
498 for gene integration consists of two 1~1.5 kb homology arms, which correspond to
499 sequences 5'-upstream and 3'-downstream of the integration site, and a loxP-URA3-
500 loxP cassette, the latter of which was used to recover the URA3 screening marker by
501 using Cre-loxP recombination system. The plasmid used for gene integration was
502 inserted into the *Y. lipolytica* chromosome for gene overexpression. Homology arms
503 of integration sites, as well as terminators and promoters, were amplified by PCR
504 using the genomic DNA from strain Po1fk or other constructed plasmids as templates.
505 The exogenous gene coding sequences were codon-optimized and synthesized by
506 Genewiz (Suzhou, China). *Y. lipolytica* endogenous gene *Yl*ACC1 (YALI0C11407g)

507 devoid of intron sequence was amplified through PCR utilizing the genomic DNA of
508 strain Po1fk as the template. The gene sequences that have been codon optimized
509 are provided in the supplementary **Table S2**. All cloning primers and check primers
510 are listed in supplementary **Table S3**.

511 **4.3 *Y. lipolytica* transformation and strain verifications**

512 The strain to be transformed was cultured in YPD medium for 24 hours, after
513 which the yeast cells were collected and resuspended in PBS buffer to wash away the
514 YPD medium. Subsequently, 50% PEG4000, 2 M lithium acetate, salmon sperm DNA,
515 and a linearized plasmid were added for homologous recombination transformation
516 (*37*). Positive clones were selected on CSM-Ura plates, and genomic DNA from the
517 clones was extracted using the Lysis Buffer with Microorganism Direct PCR Kit (Takara,
518 Beijing) for PCR-based identification. A single positive clone identified by PCR was
519 then inoculated in YPD medium for 24 hours and transformed with the pYLXP'-Cre
520 plasmid to eliminate the URA3 marker gene. The resulting colonies were streaked on
521 both YPD-5-FOA and CSM-Ura plates. Colonies that grew on YPD-5-FOA plates but
522 failed to grow on CSM-Ura plates were selected for PCR analysis to confirm the
523 successful elimination of the URA3 marker gene. Strains lacking the URA3 marker
524 gene were then subjected to another round of linearized plasmid transformation and
525 screening. All strains constructed in this work are listed in supplementary **Table S4**.

526 **4.4 Dry cell weight quantification and triacetic acid lactone extraction**

527 The cell growth was monitored by measuring the optical density at 600 nm
528 (OD600) with a UV–vis spectrophotometer that could also be converted to dry cell
529 weight (DCW) according to the calibration curve (DCW: OD600 = 0.33:1 (g/L). The
530 fermentation broth was centrifuged at 12,000 rpm for 3 min, and the culture was
531 used for analyzing the concentration of TAL. The reported titers for TAL and HHEP
532 represent the total (intracellular and extracellular) concentrations. Metabolite
533 extraction was performed by subjecting the entire culture broth, including cells, to
534 freeze-thaw cycles and mechanical grinding to ensure complete release of
535 intracellular products prior to analysis. In general, the extracellular TAL or HHEP
536 accounts for more than 85% of the production. For complete extraction of TAL, 100
537 μL fermentation culture was resuspended in 700 μL of ultrapure water containing
538 plastic particles as abrasives. The cell culture was grinded using a cryo-grinding
539 machine at -20 °C for 20 cycles of 40 s each, followed by centrifugation at 12,000 rpm
540 for 3 min. After the mixture was centrifuged, the supernatant was taken for high
541 performance liquid chromatography (HPLC) analysis.

542 **4.5 Characterization and quantification of TAL, 3-HP, and unknown peak**

543 An Agilent 1260 Infinity II instrument was utilized for HPLC analysis, with a
544 variable wavelength detector (VWD) and a C18 column (4.6 mm × 100 mm). The
545 HPLC analysis was carried out using a mobile phase consisting of solvent A (0.1%
546 formic acid in water) and solvent B (methanol). A gradient elution was applied
547 starting with 10% B, increasing to 100% B over 20 minutes, followed by 3 minutes at
548 100% B. The flow rate was 1.0 mL/min, with a column temperature of 30°C.
549 Detection was performed at 280 nm, and the injection volume was 10 µL (*38*).
550 Retention time of triacetic acid lactone is about 5.2 min. The HPLC analysis for 3-
551 hydroxypropionate (3-HP) was carried out using a single mobile phase (0.1% formic
552 acid in water - methanol (95:5, v/v) mixture), and the total elution time was 10
553 minutes. The flow rate was 1.0 mL/min, with a column temperature of 30°C.
554 Detection was performed at 210 nm for 3-HP, and the injection volume was 10 µL.
555 Retention time of 3-HP is about 3.0 min. TAL and 3-HP standard was purchased from
556 Macklin, China.

557 The unknown compound was characterized by using a Thermo Scientific Q
558 Extractive mass spectrometer equipped with an electrospray ionization (ESI) source
559 operated in both positive and negative ionization mode. Full-scan mass spectra were
560 acquired over a range of m/z 50–500. ESI parameters were optimized as follows: the
561 spray voltage 3500 V, capillary temperature 350 °C, sheath gas 30 Arb, aux gas 10 Arb,
562 probe heater temp 325 °C. Chromatographic separation was achieved using a C18
563 column (2.1 mm × 100 mm) with a flow rate of 0.5 mL/min and an injection volume
564 of 5 µL, following the same mobile phase composition and gradient elution program
565 as the HPLC method.

566 **4.6 Lipid extraction and quantification**

567 A total of 4 OD units of cell culture were collected into a centrifuge tube and
568 centrifuged to remove the supernatant. To the cell pellet, 100 µL of methyl
569 tridecanoate (C13:0 methyl ester) internal standard was added, followed by 500 µL of
570 0.5 M sodium-methanol solution. The mixture was vortexed at 1,200 rpm for 2 h.
571 Subsequently, 40 µL of 98% sulfuric acid was added to neutralize the sample. Fatty
572 acid methyl esters (FAMEs) were extracted by adding 400 µL of hexane to each
573 sample, followed by vortexing at 1,200 rpm for 10 min. The samples were then
574 centrifuged at 14,000 rpm for 2 min, and 250 µL of the hexane phase was collected,
575 the hexane phase was filtered through a 0.22 μm membrane filter and analyzed using
576 gas chromatography–flame ionization detection (GC-FID) for quantitative

determination of fatty acid content. Total lipid was calculated as the sum of the major fatty acid species detected, including C16:0, C16:1, C17:0, C17:1, C18:0, C18:1, and C18:2.

Statistical analysis of metabolite titer and content was conducted using Student's t-test, and the significances were defined as: $P > 0.05$ (ns), $P < 0.05$ (*), $P < 0.01$ (**), $P < 0.001$ (***). Each value represents the mean ± standard deviation from at least three independent experiments ($n > 3$).

Author contributions

Jinpeng Wang: Conceptualization, Investigation, Data curation, Methodology, Visualization, Writing - original draft. Yuxiang Hong: Data curation, Visualization, Investigation. Zizhao Wu: Methodology, Investigation. Ayelet Fishman: Writing - review & editing. Peng Xu: Conceptualization, Writing - review & editing, Project administration, Funding acquisition.

Data availability

Data will be made available on reasonable requests.

Acknowledgements

This work was financially supported by the National Natural Science Foundation of China (22378083), Guangdong Provincial Key Laboratory of Materials and Technologies for Energy Conversion (MATEC), and Muyuan laboratory (Program ID: 12106022401).

Table 1. Summary of the reaction components of canonical (**a**, **b**), noncanonical (**c**) and the new predicted malonyl-CoA (**d** and **e**) pathways.

Pathway		Reaction	Cofactor	ATP consume	CO_2 release	Redox balance	Enzyme	EC	Source
Canonical	a	Pyruvate + CoASH + NAD <=> Acetyl-CoA + NADH + CO2	CoASH,NAD+	0	1	NADH	PDH	1.2.1.51	Tong, L. (2005) (*16*)
		Acetyl-CoA + ATP + CO2 + H2O <=> ADP + Malonyl-CoA + Pi	NA	1	0	0	ACC	6.4.1.2	
	b	Malonate + CoASH + ATP +H2O <=> AMP + Malonyl-CoA + 2Pi	CoASH	2	0	0	MS	6.2.1.76	Wakil, S. J. (1958) (*19*)
Noncanonical	c	beta-Alanine + Pyruvate <=> alpha-Alanine + Malonate semialdehyde	NA	0	0	0	TA(BauA)	2.6.1.18	Li, J., et al. (2024) (*20*)
		Malonate semialdehyde + CoASH + NADP <=> Malonyl-CoA + NADPH	CoASH,NADP+	0	0	NADPH	MCR-C	1.2.1.75	
Predicted	d	L-glutamate + 2-oxoglutarate + O2 <=> 3-hydroxy-L-glutamate + succinate + CO2	NA	0	1	0	IboH	1.14.11.76	Obermaier, S., et al. (2020)(*21*), Nie, M., et al. (2024) (*22*)
		3-Hydroxy-L-glutamate <=> Malonate semialdehyde + Glycine	NA	0	0	0	LtaE	4.1.2.48	
		Malonate semialdehyde + CoASH + NADP <=> Malonyl-CoA + NADPH	CoASH,NADP+	0	0	NADPH	MCR-C	1.2.1.75	
	e	Aspartate <=> beta-Alanine + CO2	NA	0	1	0	ADC	4.1.1.11	Cronan, J., et al. (1980)(*23*), Yamashita, M., et al. (1996) (*24*)
		beta-Alanine + H2O+ O2 <=> Malonate semialdehyde + H2O2 + NH3	NA	0	0	0	MAO	1.4.3.21	
		Malonate semialdehyde + CoASH + NADP <=> Malonyl-CoA + NADPH	CoASH,NADP+	0	0	NADPH	MCR-C	1.2.1.75	

Table 2. Summary of thermodynamic and kinetic parameters of canonical, noncanonical and the novel malonyl-CoA pathways.

Pathway		Reaction	eQuilibrator 3.0				BRENDA		UniKP (Prediction)		
			$\Delta_rG'^m$ [kJ/mol]	$\Delta_rG'^m$(total) [kJ/mol]	$\Delta_rG'^o$ [kJ/mol]	$\Delta_rG'^o$(total) [kJ/mol]	K'_{eq}	K_m(mM)	k_{cat}(1/s)	K_m(mM)	k_{cat}/K_m(1/mMs)
Canonical	a	Pyruvate + CoA-SH + NAD <=> Acetyl-CoA + NADH + CO2	-34.2 ± 6.3	-51.3	-34.2 ± 6.4	-51.3	1.0 × 10^6	0.027 - 0.21	7.08	0.91	7.77
		Acetyl-CoA + ATP + CO2 + H2O <=> ADP + Malonyl-CoA + Pi	-17.1 ± 6.2		-17.1 ± 6.3		1.0 × 10^3	0.0002 - 1.2	4.90	0.04	123.00
	b	Malonate + CoA-SH + ATP +H2O <=> AMP + Malonyl-CoA + 2Pi	-53.4 ± 2.9	-53.4	-36.3 ± 2.9	-36.3	2.3 × 10^6	0.0368 - 8.7	5.53	0.38	14.53
Noncanonical	c	beta-Alanine + Pyruvate <=> alpha-Alanine + Malonate semialdehyde	-3.7 ± 5.7	0.6	-3.7 ± 5.7	-16.5	4	1.1 - 14	0.96	3.47	0.28
		Malonate semialdehyde + CoA-SH + NADP <=> Malonyl-CoA + NADPH	4.3 ± 8.8		-12.8 ± 8.8		1.8 × 10^2	NA	2.96	0.57	5.17
Predicted	d	L-glutamate + 2-oxoglutarate + O2 <=> 3-hydroxy-L-glutamate + succinate + CO2	-444.0 ± 10.2	-466.6	-444.0 ± 10.2	-466.6	6.7 × 10^77	NA	5.08	0.86	5.90
		3-Hydroxy-L-glutamate <=> Malonate semialdehyde + Glycine	-26.9 ± 9.2		-9.8 ± 9.2		50	NA	2.41	0.71	3.38
		Malonate semialdehyde + CoA-SH + NADP <=> Malonyl-	4.3 ± 8.8		-12.8 ± 8.8		1.8 × 10^2	NA	2.96	0.57	5.17

	CoA + NADPH									
e	Aspartate <=> beta-Alanine + CO2	-34.0 ± 11.7	-146.3	-16.9 ± 11.7	-129.2	9.1 × 10^2	0.151 - 3.18	6.90	0.57	12.09
	beta-Alanine + H2O+ O2 <=> Malonate semialdehyde + H2O2 + NH3	-116.6 ± 10.1		-99.5 ± 10.1		2.8 × 10^17	0.00088 - 12.8	12.70	0.64	19.82
	Malonate semialdehyde + CoASH + NADP <=> Malonyl-CoA + NADPH	4.3 ± 8.8		-12.8 ± 8.8		1.8 × 10^2	NA	2.96	0.57	5.17

References

1. Z. Xue *et al.*, Production of omega-3 eicosapentaenoic acid by metabolic engineering of Yarrowia lipolytica. *Nature biotechnology* **31**, 734-740 (2013).
2. K. Qiao, T. M. Wasylenko, K. Zhou, P. Xu, G. Stephanopoulos, Lipid production in Yarrowia lipolytica is maximized by engineering cytosolic redox metabolism. *Nature biotechnology* **35**, 173-177 (2017).
3. P. Xu, K. Qiao, W. S. Ahn, G. Stephanopoulos, Engineering Yarrowia lipolytica as a platform for synthesis of drop-in transportation fuels and oleochemicals. *Proceedings of the National Academy of Sciences* **113**, 10848–10853 (2016).
4. L. Milke, J. Marienhagen, Engineering intracellular malonyl-CoA availability in microbial hosts and its impact on polyketide and fatty acid synthesis. *Applied microbiology and biotechnology* **104**, 6057-6065 (2020).
5. Z. Tan, J. M. Clomburg, S. Cheong, S. Qian, R. Gonzalez, A polyketoacyl-CoA thiolase-dependent pathway for the synthesis of polyketide backbones. *Nature Catalysis* **3**, 593-603 (2020).
6. K. A. Markham *et al.*, Rewiring Yarrowia lipolytica toward triacetic acid lactone for materials generation. *Proceedings of the National Academy of Sciences* **115**, 2096-2101 (2018).
7. P. Xu, S. Ranganathan, Z. L. Fowler, C. D. Maranas, M. A. G. Koffas, Genome-scale metabolic network modeling results in minimal interventions that cooperatively force carbon flux towards malonyl-CoA. *Metabolic engineering* **13**, 578-587 (2011).
8. Y. Lv, M. Marsafari, M. Koffas, J. Zhou, P. Xu, Optimizing Oleaginous Yeast Cell

Factories for Flavonoids and Hydroxylated Flavonoids Biosynthesis. *ACS synthetic biology* **8**, 2514-2523 (2019).

9. Q. Dan *et al.*, A polyketide-based biosynthetic platform for diols, amino alcohols and hydroxy acids. *Nature Catalysis* **8**, 147-161 (2025).

10. N. Lee *et al.*, Retrobiosynthesis of unnatural lactams via reprogrammed polyketide synthase. *Nature Catalysis* **8**, 389-402 (2025).

11. W. Wang *et al.*, Harnessing the intracellular triacylglycerols for titer improvement of polyketides in Streptomyces. *Nature biotechnology* **38**, 76-83 (2020).

12. X. Luo *et al.*, Complete biosynthesis of cannabinoids and their unnatural analogues in yeast. *Nature* **567**, 123-126 (2019).

13. J. Ma, Y. Gu, P. Xu, Biosynthesis of cannabinoid precursor olivetolic acid in genetically engineered Yarrowia lipolytica. *Communications Biology* **5**, 1239 (2022).

14. W. Zha, S. B. Rubin-Pitel, Z. Shao, H. Zhao, Improving cellular malonyl-CoA level in Escherichia coli via metabolic engineering. *Metabolic engineering* **11**, 192-198 (2009).

15. A. O. Johnson *et al.*, Design and application of genetically-encoded malonyl-CoA biosensors for metabolic engineering of microbial cell factories. *Metabolic engineering* **44**, 253-264 (2017).

16. L. Tong, Acetyl-coenzyme A carboxylase: crucial metabolic enzyme and attractive target for drug discovery. *Cellular and Molecular Life Sciences CMLS* **62**, 1784-1803 (2005).

17. S. H. Klass *et al.*, Engineering controllable alteration of malonyl-CoA levels to

enhance polyketide production. *Nature Chemical Biology* **21**, 1214-1225 (2025).

18. C. E. Bowman, M. J. Wolfgang, Role of the malonyl-CoA synthetase ACSF3 in mitochondrial metabolism. *Advances in Biological Regulation* **71**, 34-40 (2019).

19. S. J. Wakil, A MALONIC ACID DERIVATIVE AS AN INTERMEDIATE IN FATTY ACID SYNTHESIS. *Journal of the American Chemical Society* **80**, 6465-6465 (1958).

20. J. Li *et al.*, A non-carboxylative route for the efficient synthesis of central metabolite malonyl-CoA and its derived products. *Nature Catalysis* **7**, 361-374 (2024).

21. S. Obermaier, M. Müller, Ibotenic Acid Biosynthesis in the Fly Agaric Is Initiated by Glutamate Hydroxylation. *Angewandte Chemie International Edition* **59**, 12432-12435 (2020).

22. M. Nie, J. Wang, K. Zhang, Engineering a Novel Acetyl-CoA Pathway for Efficient Biosynthesis of Acetyl-CoA-Derived Compounds. *ACS synthetic biology* **13**, 358-369 (2024).

23. J. E. Cronan, Beta-alanine synthesis in Escherichia coli. *Journal of Bacteriology* **141**, 1291-1297 (1980).

24. M. Yamashita *et al.*, maoB, a gene that encodes a positive regulator of the monoamine oxidase gene (maoA) in Escherichia coli. *Journal of Bacteriology* **178**, 2941-2947 (1996).

25. H. Yu, H. Deng, J. He, J. D. Keasling, X. Luo, UniKP: a unified framework for the prediction of enzyme kinetic parameters. *Nature communications* **14**, 8211 (2023).

26. M. E. Beber *et al.*, eQuilibrator 3.0: a database solution for thermodynamic constant estimation. *Nucleic Acids Research* **50**, D603-D609 (2022).

27. B. Niebel, S. Leupold, M. Heinemann, An upper limit on Gibbs energy dissipation governs cellular metabolism. *Nature Metabolism* **1**, 125-132 (2019).

28. X. Yang *et al.*, Physical bioenergetics: Energy fluxes, budgets, and constraints in cells. *Proceedings of the National Academy of Sciences* **118**, e2026786118 (2021).

29. E. Schrödinger, *What is life?: The physical aspect of the living cell.* (University Press, Dhaka, Bangladesh, 1945), pp. 1 online resource (viii, 91 pages, IV plates on 92 leaves illustrations).

30. S. Eckermann *et al.*, New pathway to polyketides in plants. *Nature* **396**, 387-390 (1998).

31. J. M. Jez *et al.*, Structural control of polyketide formation in plant-specific polyketide synthases. *Chemistry & Biology* **7**, 919-930 (2000).

32. I. Borodina *et al.*, Establishing a synthetic pathway for high-level production of 3-hydroxypropionic acid in Saccharomyces cerevisiae via β-alanine. *Metabolic engineering* **27**, 57-64 (2015).

33. A. J. Winter *et al.*, Programmed Iteration Controls the Assembly of the Nonanoic Acid Side Chain of the Antibiotic Mupirocin. *Angewandte Chemie International Edition* **61**, e202212393 (2022).

34. Y. Lv, H. Edwards, J. Zhou, P. Xu, Combining 26s rDNA and the Cre-loxP System for Iterative Gene Integration and Efficient Marker Curation in Yarrowia lipolytica. *ACS synthetic biology* **8**, 568-576 (2019).

35. L. Wong, J. Engel, E. Jin, B. Holdridge, P. Xu, YaliBricks, a versatile genetic toolkit for streamlined and rapid pathway engineering in Yarrowia lipolytica. *Metabolic*

Engineering Communications **5**, 68-77 (2017).

36. L. Wong, B. Holdridge, J. Engel, P. Xu, in *Microbial Metabolic Engineering: Methods and Protocols,* C. N. S. Santos, P. K. Ajikumar, Eds. (Springer New York, New York, NY, 2019), pp. 155-177.

37. D. C. Chen, J. M. Beckerich, C. Gaillardin, One-step transformation of the dimorphic yeast Yarrowia lipolytica. *Applied microbiology and biotechnology* **48**, 232-235 (1997).

38. H. Liu, M. Marsafari, F. Wang, L. Deng, P. Xu, Engineering acetyl-CoA metabolic shortcut for eco-friendly production of polyketides triacetic acid lactone in Yarrowia lipolytica. *Metabolic engineering* **56**, 60-68 (2019).

Figure captions

Fig. 1 Malonyl-CoA canonical, noncanonical, and predicted pathways: **(A)** Novel O_2-dependent malonyl-CoA pathways derived from L-glutamate (ILM route). IboH: 2-oxoglutarate-dependent L-glutamate dioxygenase; LtaE: aldolase; MCR-C: malonyl-CoA reductase C-terminal; **(B)** Novel O_2-dependent malonyl-CoA pathways derived from L-aspartate (AMM route). ADC: aspartate decarboxylase, MAO: monoamine oxidase; **(C)** Noncanonical TA-MCR route involves malonate semialdehyde (MalSA). TA: transaminase; **(D)** Canonical PDH-ACC route. PDH: pyruvate dehydrogenase, ACC: acetyl-CoA carboxylase.

Fig. 2 Testing the functionality of the novel malonyl-CoA pathways. (**A**) The simplest polyketide pathway encoded by 2-pyrone synthase (2-PS) was used as a reporter molecule; (**B**) Three TAL pathways, TAL-ACC, TAL-ILM, and TAL-AMM tested in this work; (**C**) TAL titer and specific TAL yield from the engineered strains in deep-well plates using YPD80 medium. Experiments were performed in triplicate, and the data is reported as mean ± SD. *** indicates statistically highly significant ($p < 0.001$), ** indicates statistically significant ($p < 0.01$), * indicates statistically significant ($p < 0.05$); (**D**) HPLC profile of TAL and an unknown by-product from the engineered strains; (**E**) LC-MS spectra of the unknown metabolite from the TAL-AMM strain.

Fig. 3. Deciphering the biosynthetic route of the nonnatural polyketide HHEP. (**A**) Biosynthetic route of TAL by 2PS. (**B**) Generation of 3-HP and 3-HP-CoA from endogenous amino acid metabolism (upper panel) and β-alanine from L-aspartate decarboxylation (lower panel). BAPAT: β-alanine-pyruvate aminotransferase; MAO: monoamine oxidase; HBD1: 3-hydroxyacyl-CoA dehydrogenase; ACS2/EHD3: 3-hydroxypropanoyl-CoA synthetase; POX1-6: Fatty-acyl-CoA oxidase; MFE2: Multifunctional β-oxidation enzyme, hydratase/dehydrogenase; ECH2: Enoyl-CoA hydratase. (**C**) 3-HP-CoA serves as a priming molecule to synthesize HHEP by 2PS. Spontaneous lactonization of triketide intermediates leads to the formation of triacetic acid lactone (**D**) and 4-hydroxy-6-hydroxyethyl-2-pyrone (**E**).

Fig. 4 Validating 3-HP as an intermediate for HHEP synthesis. (**A**) HPLC profile of 3-HP in the TAL-ACC strain with feeding of 34 mM β-alanine; (**B**) LC-MS characterization of 3-HP in the TAL-ACC strain; (**C**) Production of 3-HP in the TAL-ACC strain with or without feeding of 34 mM β-alanine in shaking flask using YPD80 medium. β-Ala feeding: 5 mM, 5 mM, 8 mM, 8 mM, and 8 mM were added at 24 h, 36 h, 48 h, 60 h, and 72 h, respectively, resulting in a total supplement of 34 mM; (**D**) Production of HHEP in the TAL-AMM strain with or without feeding of 10 mM 3-HP

in shaking flask using YPD80 medium. 3-HP feeding: 1.4 mM, 1.4 mM, 2.4 mM, 2.4 mM, and 2.4 mM were added at 24 h, 36 h, 48 h, 60 h, and 72 h, respectively, resulting in a total supplement of 10 mM. L-Aspartate feeding: 5 mM, 5 mM, 8 mM, 8 mM, and 8 mM were added at 24 h, 36 h, 48 h, 60 h, and 72 h, respectively, resulting in a total supplement of 34 mM; (**E**) TAL and HHEP production in the TAL-A and TAL-AMM strain after 48 hours of fermentation in deep-well plates using YPD80 medium. TAL-A is the strain with expression of 2PS and ADC. TAL-AMM is the strain with expression of 2PS and the entire AMM pathway.

Fig. 5. Feeding L-glutamate or L-aspartate to improve polyketide production in TAL-ILM or TAL-AMM strain. (**A**) TAL, HHEP and 3-HP production in TAL-ILM strain with or without feeding 34 mM L-glutamate in 250 mL baffled-flask using YPD80 medium. L-Glutamate feeding: 5 mM, 5 mM, 8 mM, 8 mM, and 8 mM were added at 24 h, 36 h, 48 h, 60 h, and 72 h, respectively, resulting in a total supplement of 34 mM; (**B**) Growth fitness of HHEP-producing strain (TAL-AMM) is reduced compared to other TAL-producing strain; (**C**) TAL, HHEP and 3-HP production in TAL-AMM strain with or without feeding of 34 mM L-aspartate in 250 mL baffled-flask using YPD80 medium. L-Aspartate feeding: 5 mM, 5 mM, 8 mM, 8 mM, and 8 mM were added at 24 h, 36 h, 48 h, 60 h, and 72 h, respectively, resulting in a total supplement of 34 mM; (**D**) HPLC profile show that the HHEP peak returned to basal level almost undetectable when HBD1 gene was deleted; (**E**) Production of HHEP in the TAL-ΔHBD1-AMM strain with or without feeding of 60 g/L peptone in shaking flask using YPD80 medium. Peptone feeding: 10 g/L, 10 g/L, 10 g/L, 15 g/L, and 15 g/L were added at 24 h, 36 h, 48 h, 60 h, and 72 h, respectively, resulting in a total supplement of 60 g/L; (**F**) HPLC profile of TAL and HHEP from the engineered strains after knocking out HBD1: the product shifts to TAL accumulation; (**G**) TAL titer, specific TAL yield, lipid titer and lipid content from the engineered strains with or without amino acid feeding in 250 mL baffled-flask using YPD80 medium. L-Glutamate or L-aspartate feeding: 5 mM, 5 mM, 8 mM, 8 mM, and 8 mM were added at 24 h, 36 h, 48 h, 60 h, and 72 h, respectively, resulting in a total supplement of 34 mM. Experiments were performed in triplicate, and the data is reported as mean ± SD. *** indicates statistically highly significant ($p < 0.001$), * indicates statistically significant ($p < 0.05$), ns indicates statistically significant ($p > 0.05$).

Fig. 6 Feeding L-aspartate to improve polyketide and lipid production in TAL-AMM strain in a 1.0 L mini-bioreactor. TAL+HHEP(**A**), HHEP(**B**), TAL(**C**) and 3-HP(**D**) production in TAL-AMM strain with or without feeding of 100 mM L-aspartate in a 1L bioreactor. L-Aspartate feeding: 5 mM, 10 mM, 15 mM, 15 mM, 15 mM, 20 mM, and 20 mM were added at 0 h, 12 h, 24 h, 36 h, 48 h, 60 h, and 72 h, respectively,

resulting in a total supplement of 100 mM; (**E**) Optical density OD600 during fermentation in a 1L bioreactor; (**F**) Amount of glucose consumed during fermentation in a 1L bioreactor; Total Lipid titer (**G**), lipid content (**H**) and total odd-chain fatty acid (OCFA) production in TAL-AMM strain with or without feeding of 100 mM L-aspartate in a 1L bioreactor.